Numerical determination of a low relaxation time Oldroyd-B polymer solution

Guillaume Maîtrejean
Laboratoire Rhéologie et Procédés
Univ. Grenoble Alpes, LRP
F-38000 Grenoble France
Email: guillaume.maitrejean@univ-grenoble-alpes.fr

Maxime Rosello
Laboratoire Rhéologie et Procédés
Univ. Grenoble Alpes, LRP
F-38000 Grenoble France

Denis CD Roux
Laboratoire Rhéologie et Procédés
Univ. Grenoble Alpes, LRP
F-38000 Grenoble France

Pascal Jay
Laboratoire Rhéologie et Procédés
Univ. Grenoble Alpes, LRP
F-38000 Grenoble
France

Jean Xing
Markem-Imaje Industries
ZA de l'Armailler 9
rue Gaspard Monge
BP 110 26501 Bourg-Lés-Valence
France

Bruno Barbet
Markem-Imaje Industries
ZA de l'Armailler 9
rue Gaspard Monge
BP 110 26501 Bourg-Lés-Valence
France

For very low relaxation time (i.e. lower than a microsecond) viscoelastic fluid experimental determination is difficult, if not impossible. In the present work the relaxation time measurement of a weakly elastic polymer solution used in industrial CIJ is done by comparing drop shapes obtained both numerically and experimentally. The numerical simulations use a viscoelastic Oldroyd-B model which relaxation time is fitted using experimental results. That kind of numerical rheometry is particularly convenient for weakly elastic solution physical parameters which can not be measured by experimental means.

1 Introduction

Capillary breakup phenomena have a wide range of applications from ink-jet printing to DNA sampling. In micro jetting devices, polymer solutions often experience non Newtonian behavior which greatly influence breakup dynamics. Drops generation from non Newtonian fluid jets breakup is a well known topic which has already been addressed both numerically and experimentally [1–3]. Elastic and viscous effects are known to have a great influence on the breakup dynamics. More precisely, they are known to delay the onset of the jet breakup [4, 5]. In the present work, the relaxation time of a weakly elastic ink used in industrial continuous ink-jet printing (CIJ) devices is determined. This ink is a low viscosity dilute polymer with high polydispersity. A first estimation of the elastic relaxation time is calculated using Zimm theory [6], and is found to be out of the measurement range of both extensional rheometry (ROJER [7]) or microfluidic devices [8]. As a result, an original approach is introduced to determine the relaxation time, relying on the comparison of capillary breakup shapes between numerical simulations and experiments.

2 Experimental setup and jets

The experimental device is similar to the one used for ROJER extensional rheometry measurements [2] (see figure 1). The flow is generated by a pump and the jet is created using a micro-nozzle. Then, it is strobed at a given frequency and synchronized with the drive frequency ($10kHz < f_d < 100kHz$) in order to display a static image (1024×778 pixels with $1px \approx 1\mu m$). The visualization software is ImageXpert.

In the present work, the fluid jets have been generated experimentally with the same device at stimulation amplitudes ranging from 2V to 62V and with a constant dimensionless wave number $x = 0.6$, where x writes:

$$x = 2\pi R_0 \frac{v}{f} \tag{1}$$

with R_0 the radius of the unperturbed jet, v the jet velocity

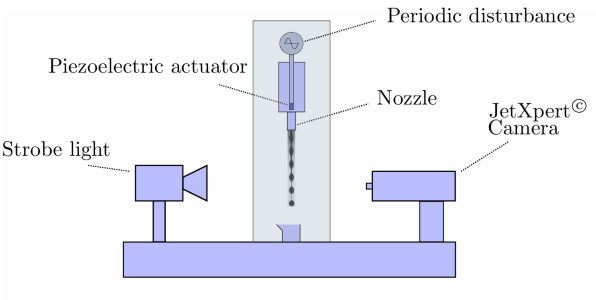

Fig. 1

and f the stimulation frequency.

Reynolds and Ohnesorge numbers of the jet, are

$$Re = \rho v R_0/\eta_0 = 110 \tag{2}$$

and

$$Oh = \eta_0/\sqrt{\rho R_0 \sigma} = 0.2 \tag{3}$$

respectively. They are calculated for undisturbed jets and are constant for every disturbance amplitudes.

Figure 2 depicts the jet morphologies after jetting the weakly elastic ink. The jets have been pictured at the breakup distance from the nozzle for stimulation amplitudes ranging from 2 to $62V$. For small stimulation amplitude (left of the figure), drop shape remains almost the same in the linear regime of stimulation, i.e. where stimulation is lower than $15V$. In that regime we also observe a forward-merging satellite.For higher stimulation amplitude, no satellite can be observed anymore and a thread links the first droplets to the unbroken jet. This thread is typical of breakup of weakly elastic polymer strain hardening solutions [9].

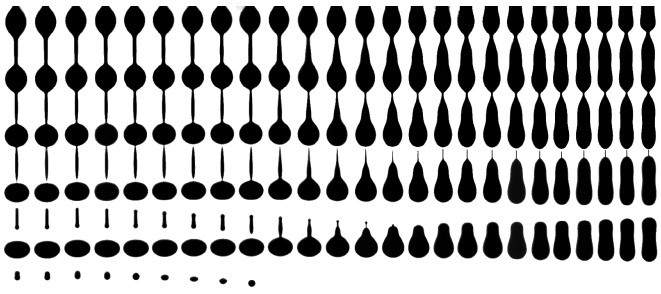

Fig. 2: Breakup shapes of the polymer solution for stimulation amplitudes ranging from 2V (left) to 62V (right).

Figure 3 shows the breakup length as a function of the disturbance amplitude, i.e. as a function of the tension applied to the piezoelectric actuator. The so-called breakup length, also called "intact length" and noted $\mathcal{L}^b_{exp}$ hereafter, has been widely studied both in linear and non-linear regime, (see [10] and therein references) and is directly linked to the nozzle outlet velocity disturbance [11, 12]. As expected a quasi-linear regime is observed for low amplitude stimulation and (lower than $15V$) which is in agreement with the previous observation about the drop shapes. The breakup length decreases with the disturbance amplitude and seems to reach a minimum length for $62V$.

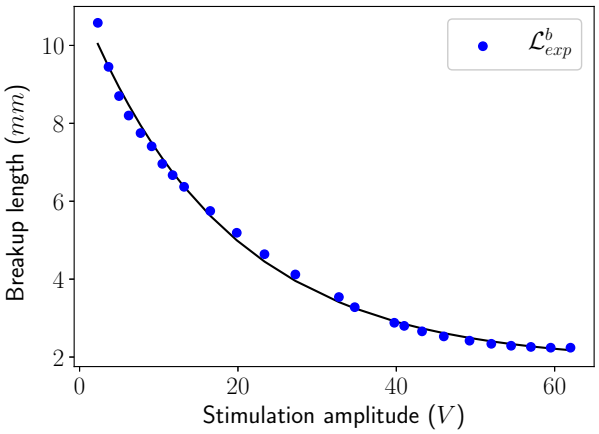

Fig. 3: Experimental breakup lengths $\mathcal{L}^b_{exp}$ for the weak elastic ink studied in the present work.

2.1 Rheological characterization

The density $\rho = 873 kg.m^{-3}$ and the surface tension $\sigma = 22.8 mN.m^{-1}$ of the fluid have been carefully measured using an Lovis 2000MME device from Anton Paar and a MPT2 from Lauda, respectively.

The shear viscosity is measured using both ARG-2 from TA-Instruments for low shear rates ($\dot{\gamma} < 1000 s^{-1}$) and m-VROC from RheoSense for high shear rates ($1000 s^{-1} < \dot{\gamma} < 10^6 s^{-1}$). As we can see on figure 4, the viscosity shows a slight shear-thinning behavior around $10^6 s^{-1}$, but considering the incertitude of measure, the fluid viscosity is assumed constant over the full range of shear rate.

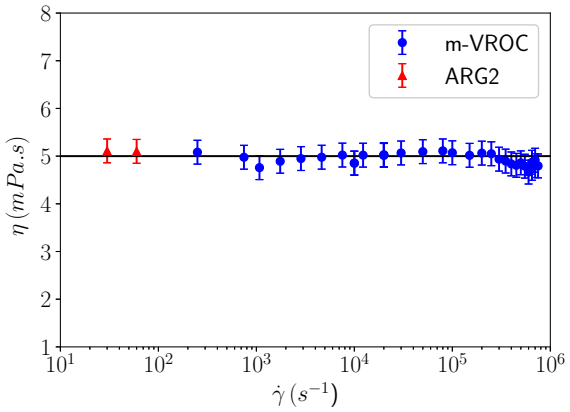

Fig. 4: Dynamic viscosity of the present polymer solution as a function of the shear rate.

As stated in the previous section, the present ink is a weakly elastic polymer solution. Zimm theory [6] can thus be used to describe polymer relaxation dynamics considering hydrodynamic interactions between chains and solvent. Zimm's theory is based on an elastic dumbbell model: it takes into account the hydrodynamic interactions between solvent and polymers but not the frictional interactions between chains. The only interaction between the modelled chains are thus are thus long range interaction, i.e. mediated by the solvent. This theory is particularly accurate for dilute polymer solutions and enables the calculation of a relaxation time τ_Z , such as :

$$\tau_Z = \frac{\eta_s[\eta]M}{RT} = 0.4\mu s \tag{4}$$

with η_s the solvent viscosity in $Pa.s$, $[\eta]$ the intrinsic viscosity in $m^3.kg^{-1}$, M_w the polymer molecular mass $kg.mol^{-1}$, R the universal gas constant and T the temperature in K.

τ_Z is an estimated, analytical relaxation time based on to main assumptions which are the monodispersity of the solution and only long-range interaction between polymer chains. However, as the present ink is unlikely to meet these criteria and particularly the monodisperse assumption, this time is a lower bound.

Let us now consider the capillary time τ_c , given by :

$$\tau_C = \sqrt{\rho R_0^3/\sigma} \tag{5}$$

with R_0 the unperturbed jet radius.

As the polymer relaxation time predicted by Zimm's theory is very small compared with the capillary time scale, the elasticity should have a negligible influence on the breakup dynamics for small to moderate stimulation amplitude. Moreover, this low relaxation $\tau_Z << \tau_C$ time prevent us from using the jetting device as a ROJER [7] in order to measure the relaxation time.

To the knowledge of the authors, no experimental device can capture such a short relaxation time and we follow another route in section 4 by comparing numerical simulation to experimental results in order to determine it. The numerical model is carefully assessed and calibrated in the next section using both a simple test case and the simulation of a Newtonian fluid jet.

3 Validation of the numerical model

The computation is performed using OpenFoam® and more specifically with its multiphase solver interFoam [13]. In order to evaluate the ability of the solver to numerically model the jetting of a non-Newtonian fluid, it is first assessed on the well-known capillary instability growth of a Newtonian fluid and eventually jetting of Newtonian fluid is considered.

3.1 Simulation of the capillary instability growth

First, the performance of the interFoam solver is assessed by simulating the growth of a perturbation at the surface of 2-dimensional axisymmetric Newtonian liquid column. The results is then be compared to the linear theory initially derived by Rayleigh [4] and then enhanced by [14], which provides well-known test case [15, 16]. The analytical dispersion equation from [14] writes:

$$\gamma\tau_c = \sqrt{\frac{1}{2}(x^2 - x^4) + \frac{9}{4}Oh^2x^4} - \frac{3}{2}Ohx^2, \tag{6}$$

with γ the growth rate, τ_c the capillary time, x the dimensionless wave number and Oh the Ohnesorge number

Simulation of the capillary instability growth consists in an axisymmetric flow within a rectangular domain of width λ and height h, and composed of a liquid of radius R_0 and a gaz. At $t = 0s$ the liquid is at rest and a small perturbation of wavelength λ and amplitude δ is applied to its surface. Domain is meshed with square elements of side Δ_x and simulation is found to converge with $\Delta_x < 7\,10^{-5}m$. Parameters of the simulation are summed up Table 1 and Fig 5 shows numerical results at different time $t \in [0s, 2s]$.

Comparison of theoretical growth rate from Eq. 6 with numerical results Fig. 6 shows excellent agreement as analytical solution is based on linearized approach whereas interFoam solves full Navier-Stokes equation.

3.2 Numerical simulation of Newtonian CIJ

In order to fine tune the numerical model for CIJ cases, jetting of a Newtonian solution of water and glycerol is addressed. The experimental set-up is identical to the one that has been used to jet the weakly elastic ink in section 2. The density, viscosity and surface tension of the solution has been carefully measured using, respectively, an Anton Paar DMA4500, an Anton Paar Lovis 2000MME and a Lauda MPT-2. Table 2 sums up the physical properties of the solution used in the numerical simulation.

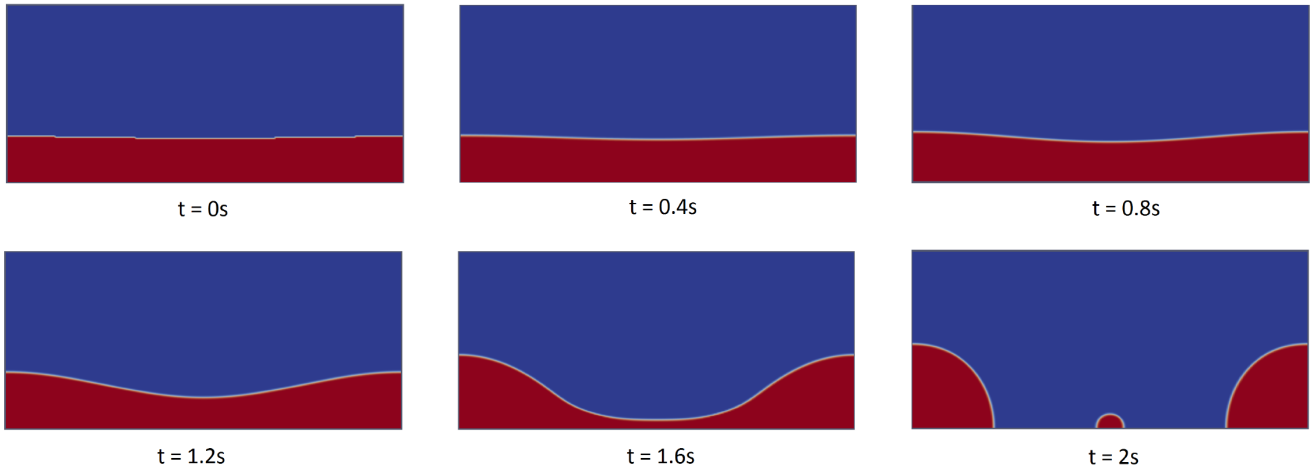

Fig. 5: Evolution of the capillary instability (liquid in red and gaz in blue)

$\rho_l(kg.m^{-3})$	1000
$\rho_g(kg.m^{-3})$	1
$\nu_l(Pa.s)$	10^{-3}
$\nu_g(Pa.s)$	10^{-6}
$h(m)$	$28\,10^{-4}$
$\lambda(m)$	$64\,10^{-4}$
$R_0(m)$	$7.07\,10^{-4}$
$\delta(m)$	$1.6\,10^{-5}$
Oh	0.2
$\tau_c(s)$	0.1
$\Delta_x(m)$	$7\,10^{-5}$

Table 1: Parameters of capillary instability simulations.

$\rho_l(kg.m^{-3})$	1128.88
$\nu_l(mPa.s)$	6.4
$\sigma(mN.m^{-1})$	69.16

Table 2: Physical parameters of glycerol + water solution.

Figure 7(a-i) shows experimental jets pictured at the breakup distance from the nozzle for stimulation amplitudes ranging from 1 to 55V

The numerical model of the CIJ device takes advantage of the axisymmetry of the problem the upper part of the numerical domain, which is thus 2-dimensional and includes fluid tank and nozzle, is depicted Fig. 8.

At $t = 0s$, both tank and nozzle are filled with fluid and the rest of the domain is filled with air. In order to jet the fluid, a pressure Dirichlet boundary condition is applied on

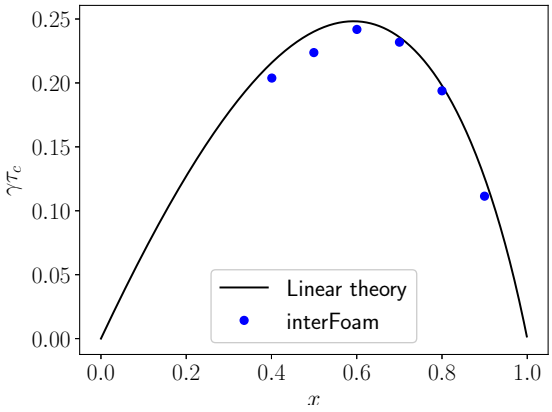

Fig. 6: Growth rate $\gamma\tau_c$ as a function of of the dimensionless wave number x

the inlet of the domain (left side of the tank) such as:

$$P = P_{tank} + P_{stim}\cos(2\pi ft) \tag{7}$$

where P_{tank} and P_{stim} are related, respectively, to the absolute steady pressure in the fluid tank, driving the jetting velocity of the fluid, and the amplitude of stimulation.

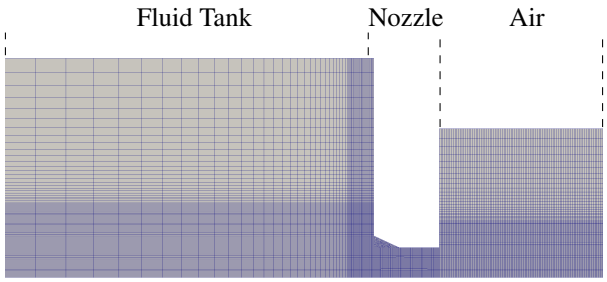

Fig. 8: Converged mesh of the tank, nozzle and nozzle outlet of the axisymmetric numerical model.

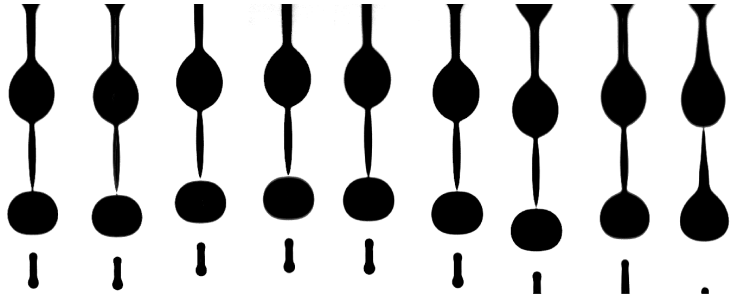

Fig. 7: Experimental jets for different stimulation amplitude (in Volts) located a the breakup length.

To accurately determine P_{tank}, P_stim is set to zero, i.e. resulting in unperturbed jet of glycerol, and both the mass flow and the dimensionless wave number x are experimentally measured and compared to numerical results by try and error process . In the present case the P_{tank} has been found $P_{tank} = 4140 mbar$.

P_{stim} is directly related to the tension applied to the piezoelectric actuator and there is no direct relation between the amplitude of stimulation in Volt and the one in Pascal. In order to determine the pressure exerted on the fluid by the piezoelectric device, i.e. P_{stim}, as a function of the tension applied T_{stim}, we must compare experimental and numerical breakup jets. One way to do so lies in comparing droplet shapes, but in this present case and due to the hight tension surface exhibited by the glycerol solution, the droplets created looks very similar (see Fig. 7) and one can not use this criterion to discriminate the jets. We then use the breakup lengths of the jets, respectively, $\mathcal{L}^b_{exp}$ and $\mathcal{L}^b_{num}$, to assess the relation between P_{stim} and T_{stim}.

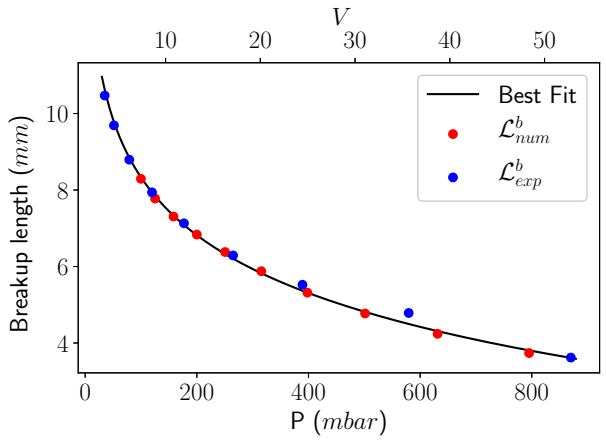

Fig. 9: Numerical and Experimental breakup lengths for glycerol solution.

Figure 9 shows both $\mathcal{L}^b_{exp}$ and $\mathcal{L}^b_{num}$ and an excellent agreement can be found between P_{stim} and T_{stim}:

$$P_{stim} = 36.4\, T_{stim}^{0.792} \tag{8}$$

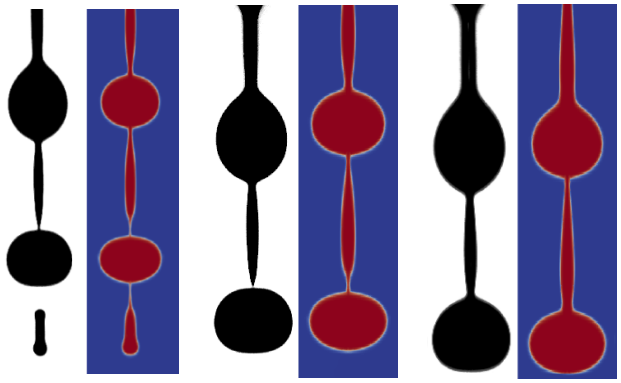

(a) 1.6V - 53$mbar$ (b) 12.2V - 264$mbar$ (c) 33V - 580$mbar$

Fig. 10: Comparison between experimental (black and white) and numerical (colour) droplet shapes for different amplitudes of stimulation

It is worth pointing out that the numerical breakup length can strongly impacted by the mesh as $\mathcal{L}^b_{num}$ relates to the length where fluid thread thickness tends towards zero. However the high surface tension exhibited by the glycerol solution prevent $\mathcal{L}^b_{num}$ to diverge from $\mathcal{L}^b_{exp}$ and excellent agreement is found between them both.

Droplet shapes depicted 10(a-c) shows also an excellent agreement between numerical and experimental results and satellites dynamic is also captured by the numerical model from low (1.6V) to high amplitude stimulations (33V).

4 Numerical determination of the relaxation time

This section focuses on the determination of the relaxation time of the weakly elastic ink presented section 2. The numerical simulation is performed using the previously fine-tuned interFoam solver (see previous subsection 3.2) and the same 2D-axisymmetric geometry.

Neither shear thinning nor strain thickening behavior is expected, thus the Oldroyd-B viscoelastic model [17] is assumed to accurately describe the viscoelastic behavior of the present weakly elastic ink.

The solvent and polymer contribution to viscosity, respectively η_s and η_p have been carefully measured and the influence of the relaxation time τ_e onto the breakup shape is investigated. Giving the value $\tau_Z = 0.4\mu s$ found in section 2.1 using Zimm's theory, τ_e from $0.5\mu s$ to $1\mu s$ will be tested.

The relaxation time has an influence on the average jet velocity v : the more elastic the fluid, the slower the jet. Thus, the instability wave number x (see 1) increases when τ_e increases. Consequently P_{tank} depends on τ_e and has been determined by ensuring a constant dimensionless wave number $x = 0.6$ for unperturbed viscoelastic jets (i.e. setting $P_{stim} = 0$ in eq. 7). Figure 11 shows the linear relation found between P_{tank} and the fluid relaxation time in order to get $x = 0.6$.

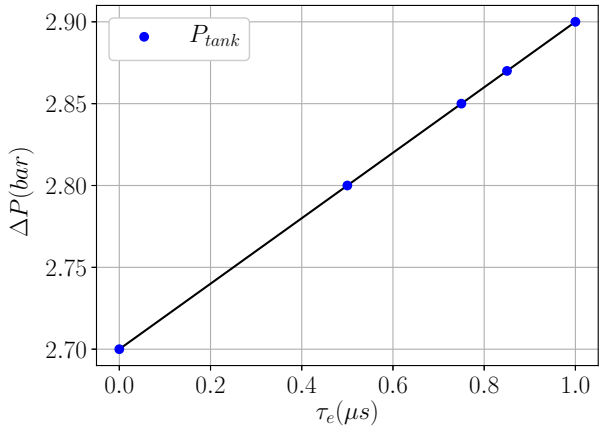

Fig. 11: P_{tank} as function of τ_e ensuring a constant dimensionless wave number $x = 0.6$ for unperturbed viscoelastic jets.

It is worth pointing out that over the studied range of relaxation times, the jet does not exhibit die-swell effect at the nozzle exit : the dependence of R_0 with τ_e is then assumed negligible, and, consequently, P_{tank} only influences the value of the jet averaged velocity v. Moreover Figure 12 presents the axial velocity profile at the nozzle outlet obtained for $\tau_e = 0\mu s$ (Newtonian), $\tau_e = 0.5\mu s$ and $\tau_e = 1\mu s$ for a jet without disturbance. It seems that within the studied relaxation time range, elasticity has a small influence onto velocity profiles.

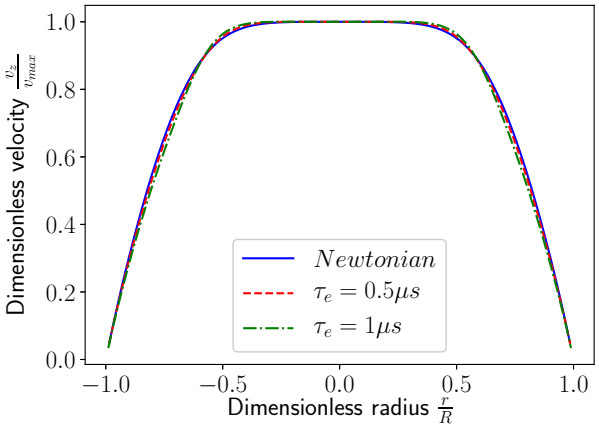

Fig. 12: Computational axial velocity profiles at the nozzle exit for the Newtonian and Oldroyd-B ($\tau_e = 0.5\mu s$ and $\tau_e = 1\mu s$) fluid jets.

From now on, a disturbance is applied to the jet using the pressure boundary condition (see eq. 7). In order to compare the numerical results to the experimental ones, one must find the relation between P_{stim} and V_{stim}, which denote, respectively, the numerical and experimental disturbance amplitudes. In section 3.2 the correlation has been found based on the breakup length.

However, as previously stated, the breakup length criterion is not fully appropriate for low to moderate surface tension fluids as the mesh has an outstanding influence on it. The results are thus compared using both the breakup length and the breakup shape which, the later being far less influenced by the mesh and thus is a good additional criterion.

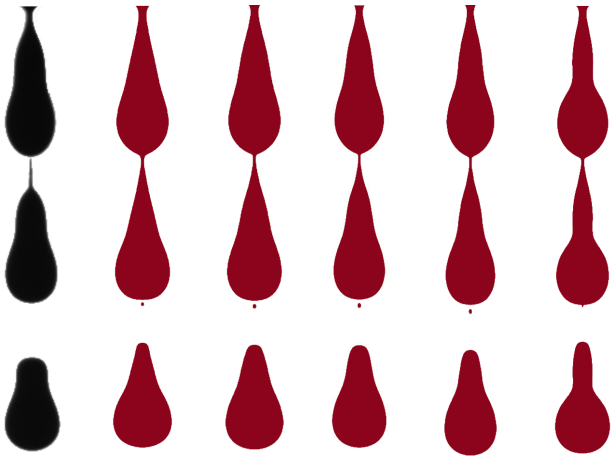

(a) 34.8V (b) Newtonian (c) $0.5\mu s$ (d) $0.75\mu s$ (e) $0.85\mu s$ (f) $1\mu s$

Fig. 13: Breakup shapes for $P_{stim} = 0.3 \cdot P_{tank}$ for both experimental (black) and numerical (red) fluids.

For each numerical fluid, i.e. Newtonian and Oldroyd-B

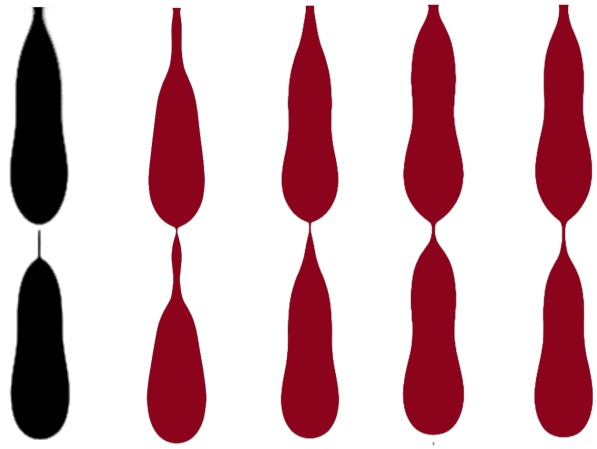

(a) $54.5V$ (b) Newtonian (c) $0.5\mu s$ (d) $0.75\mu s$ (e) $0.85\mu s$

Fig. 14: Breakup shapes for $P_{stim} = 0.5 \cdot P_{tank}$ for both experimental (black) and numerical (red) fluids.

with $\tau_e \in \{0.5, 0.75, 0.85, 1\}$, calculations are made for two values of P_{stim}, $P_{stim} = 0.3 \cdot P_{tank}$ and $P_{stim} = 0.5 \cdot P_{tank}$.

Figure 13 presents results obtained for $P_{stim} = 0.3 \cdot P_{tank}$ for every numerical fluid and with the best experimental math. From these first results, either $\tau_e = 0.75\mu s$ or $\tau_e = 0.75\mu s$ are potential candidates by matching the best experimental drop shape obtained with a disturbance amplitude of $54.5V$. While results lie in the non linear regime (see Fig. 3) the influence of the relaxation time has a moderate effect onto the drop shapes.

However when comparing the breakup length $\mathcal{L}_b^{0.3}$ we observe a strong influence of the relaxation time and, as expected, some discrepancies between the candidates and the experimental lengths which are shorter.

Figure 14 presents results for $P_{stim} = 0.3 \cdot P_{tank}$. In this case, the Newtonian case and the Oldroyd-B model at $\tau_e = 0.5\mu s$ both exhibit significant shape differences compared to the experimental case. The computation for $\tau_e = 1\mu s$ is not presented as a breakup inversion occurs, and as a result, the jet breaks up outside the numerical domain, i.e. at a length greater than $6.5mm$. Again, relation time of $\tau_e = 0.75\mu s$ and $\tau_e = 0.85\mu s$ give the most accurate breakup shapes, as already observed for $P_{stim} = 0.3 \cdot P_{tank}$.

Small differences between numerical and experimental drop shapes may due both to non linear viscoelastic effects that are not taken into account in the Oldroyd-B model and experimental uncertainties.

Fluids	$\mathcal{L}_b^{0.3}\,(mm)$	$\mathcal{L}_b^{0.5}\,(mm)$
Experimental	3.28	2.29
Newtonian	2.85	2.54
$\tau_e = 0.5\mu s$	3.3	2.25
$\tau_e = 0.75\mu s$	3.95	2.85
$\tau_e = 0.85\mu s$	4.45	4.25
$\tau_e = 1\mu s$	5.5	> 6.5

Table 3: Breakup lengths $\mathcal{L}_b^{0.3}$ and $\mathcal{L}_b^{0.5}$ of the numerical and experimental fluids.

As we can see, small changes in the polymer relaxation time τ_E have a great influence on the breakup morphology of Rayleigh-Plateau jet instability. The present work allowed us to determine a tiny range for the longest relaxation time with a precision of $10^{-7}s$. The numerically measured relaxation time $\tau_e = 0.75 - 0.85\mu s$ is coherent with Zimm predictions even if it is slightly higher ($\tau_Z = 0.4\mu s$). The small difference between analytical and computational results may due to polydispersity of the polymer solution as τ_Z is calculated using the averaged molecular mass M_w , although some polymer chains in the present solution have higher molecular mass which increase the solution relaxation time.

5 Conclusion

This original approach allows to determine the rheological properties of low viscosity and weakly viscoelastic polymer solution that can not be addressed by any experimental measurement method. Based on a trial-and-error technique, it relies on the strong dependency of the pinching curvature onto the viscoelastic relaxation time at high disturbance amplitude. However, this approach rely on an accurate numerical description of the physics at play in the process. The rheological model used must be carefully chosen to adequately model the experimental fluid.

References

[1] Morrison, N. F., and Harlen, O. G., 2011. "Inkjet printing of non-newtonian fluids". In NIP & Digital Fabrication Conference, Vol. 2011, Society for Imaging Science and Technology, pp. 360–364.

[2] Rodríguez-Rivero, C., Del Valle, E. M., and Galán, M. A., 2015. "Experimental and linear analysis for the instability of non-n ewtonian liquid jets issuing from a pressurized vibrating nozzle". *AIChE Journal,* **61**(6), pp. 2070–2078.

[3] McIlroy, C., Harlen, O., and Morrison, N., 2013. "Modelling the jetting of dilute polymer solutions in drop-on-demand inkjet printing". *Journal of Non-Newtonian Fluid Mechanics,* **201**, pp. 17–28.

[4] Rayleigh, L., 1892. "Xvi. on the instability of a cylinder of viscous liquid under capillary force". *The London, Edinburgh, and Dublin Philosophical Magazine and Journal of Science,* **34**(207), pp. 145–154.

[5] Gordon, M., Yerushalmi, J., and Shinnar, R., 1973. "Instability of jets of non-newtonian fluids". *Transactions of The Society of Rheology (1957-1977),* **17**(2), pp. 303–324.

[6] Zimm, B. H., 1956. "Dynamics of polymer molecules in dilute solution: viscoelasticity, flow birefringence and dielectric loss". *The journal of chemical physics,* **24**(2), pp. 269–278.

[7] Keshavarz, B., Sharma, V., Houze, E. C., Koerner, M. R., Moore, J. R., Cotts, P. M., Threlfall-Holmes, P., and McKinley, G. H., 2015. "Studying the effects of elongational properties on atomization of weakly viscoelastic solutions using rayleigh ohnesorge jetting extensional rheometry (rojer)". *Journal of Non-Newtonian Fluid Mechanics,* **222**, pp. 171–189.

[8] Galindo-Rosales, F. J., Alves, M., and Oliveira, M. S., 2013. "Microdevices for extensional rheometry of low viscosity elastic liquids: a review". *Microfluidics and nanofluidics,* **14**(1-2), pp. 1–19.

[9] Christanti, Y., and Walker, L. M., 2002. "Effect of fluid relaxation time of dilute polymer solutions on jet breakup due to a forced disturbance". *Journal of Rheology (1978-present),* **46**(3), pp. 733–748.

[10] Eggers, J., and Villermaux, E., 2008. "Physics of liquid jets". *Reports on progress in physics,* **71**(3), p. 036601.

[11] Pimbley, W., and Lee, H., 1977. "Satellite droplet formation in a liquid jet". *IBM Journal of Research and Development,* **21**(1), pp. 21–30.

[12] Rosello, M., Maîtrejean, G., Roux, D. C., Jay, P., Barbet, B., and Xing, J., 2018. "Influence of the nozzle shape on the breakup behavior of continuous ink jets". *Journal of Fluids Engineering,* **140**(3).

[13] Deshpande, S. S., Anumolu, L., and Trujillo, M. F., 2012. "Evaluating the performance of the two-phase flow solver interfoam". *Computational science & discovery,* **5**(1), p. 014016.

[14] Chandrasekhar, S., 2013. *Hydrodynamic and hydromagnetic stability*. Courier Corporation.

[15] Delteil, J., Vincent, S., Erriguible, A., and Subra-Paternault, P., 2011. "Numerical investigations in rayleigh breakup of round liquid jets with vof methods". *Computers & Fluids,* **50**(1), pp. 10–23.

[16] Cervone, A., Manservisi, S., and Scardovelli, R., 2010. "Simulation of axisymmetric jets with a finite element navier–stokes solver and a multilevel vof approach". *Journal of Computational Physics,* **229**(19), pp. 6853–6873.

[17] Oldroyd, J., 1950. "On the formulation of rheological equations of state". In Proceedings of the Royal Society of London A: Mathematical, Physical and Engineering Sciences, Vol. 200, The Royal Society, pp. 523–541.